PCCP

Zero-point energy constraints in RRKM and non-RRKM molecules

Drew A. McCormack†[a] and Kieran F. Lim*[b]

[a] *School of Chemistry, University of Melbourne, Parkville, Victoria 3052, Australia*
[b] *School of Biological and Chemical Sciences, Deakin University, Geelong, Victoria 3217, Australia. E-mail: lim@deakin.edu.au*

Received 15th October 1998, Accepted 2nd November 1998

The TRAPZ method for zero-point energy (ZPE) preservation (Lim and McCormack, *J. Chem. Phys.*, 1995, **102**, 1705) is generalised to molecular systems of non-zero angular momentum. The method is shown to conserve linear momentum, angular momentum and total energy. It is also found to preserve the intrinsic Rice–Ramsperger–Kassel–Marcus (RRKM) behaviour of a dissociating Al_3 cluster. The TRAPZ rate coefficients are lower than those calculated for classical ensembles, since regions of phase space with less than ZPE can no longer react. As required, the RRKM rate coefficients are upper bounds to the TRAPZ rate coefficients. The TRAPZ reaction threshold is higher than the classical (asymptotic-limit) product ZPE due to fluctuations in instantaneous normal mode ZPEs. Rotationally hot Al_2 is produced as Al_3 ZPE bending motion is converted to Al_2 angular momentum. The TRAPZ method does not preserve the non-RRKM behaviour of HNC isomerisation.

I. Introduction

Whilst it is generally preferable, in the study of molecular dynamics, to implement a quantum or semi-classical scheme, it is often impractical, or impossible, due to the computational effort required by these methods. Quasi-classical techniques, whilst not as physically desirable, are a feasible option, and there are many well documented cases where they have been used effectively to determine qualitative, and quantitative, trends of processes such as intramolecular vibrational relaxation (IVR),[1–6] collisional energy transfer (CET),[7–12] and reaction.[13–21]

The 'ZPE problem', or 'ZPE leak', has been the subject of much discussion of late, and has yet to be resolved adequately. The problem itself, that classical mechanics fails to restrict energy flow in order to preserve quantum ZPE in vibrational modes, has been well documented by many authors.[20–28] Particularly good reviews, of the problem and attempts to solve it, can be found in ref. 26 and 28. Remedies have traditionally fallen into two categories: 'passive' and 'active'.[26,28] Passive methods do not alter the classical trajectories themselves but, instead, re-interpret the results of such trajectories to account for ZPE leak.[18,21,29–31] Active methods make some modification to the equations of motion in order to assure preservation of ZPE.[20,22,25–27,32]

This paper aims to develop and test the TRAPZ (trajectory projection onto ZPE orbit) active method.[27,33,34] This technique has previously only been fully applied to the Hénon–Heiles Hamiltonian,[35] and was found to exhibit some unusual behaviour.[27,34] The dynamics of the classical Hénon–Heiles system have been well documented, and consist basically of quasi-periodic behaviour at energies below a critical value, and predominantly chaotic behaviour at higher levels.[36–42] The TRAPZ method was found to preserve the quasi-periodic behaviour at low energies, but also incite it above the critical threshold.[27] (Note that unpublished studies of other variations of TRAPZ show no signs of this effect.)[43] Our purpose is thus, in part, to determine whether this regularisation of chaotic dynamics will carry over to other systems, and also to establish whether intrinsically non-chaotic behaviour is preserved by the method.

Peslherbe *et al.* have shown that the classical rotationally cold Al_3 cluster, at energies up to 2.0 kcal mol^{-1} (8.4 kJ mol^{-1}) above the classical dissociation threshold, exhibits single-exponential decay

$$Al_3 \rightarrow Al_2 + Al \quad (1)$$

and is consistent with ergodic behaviour characteristic of RRKM systems.[44] More recently, they have performed a detailed comparison of constrained trajectory calculations,[45] utilising the active constraint referred to here as the 'Bowman–Miller–Hase' (BMH) method (elsewhere as the 'momentum-reversal' method),[22,24,26,32,45–48] with various variational RRKM and phase space theories for dissociation rate calculations of Al_3. The BMH trajectory rate coefficients were in poor agreement with those determined by RRKM theory.[45] They surmised that this was partially due to some trajectories being temporarily trapped in the 'forbidden region' of phase space by a flaw in the BMH method. Nevertheless, the BMH method maintains the ergodic nature of the molecule,[45] which is not surprising, since other studies have shown the method increases the degree of chaos, and hence the ergodicity of a system.[27,28,46,48] In contrast, some variants of the TRAPZ method have been seen to transform ergodic systems into non-ergodic ones.[27]

Studies by Chan, Shen and Pritchard on the isomerisation of HNC,[48,49]

$$HNC \rightarrow HCN \quad (2)$$

have indicated that reaction (2) does not show RRKM-type decay. However, application of a BMH-like method induced

† Present address: Leiden Institute of Chemistry, Leiden University, The Netherlands

ergodic behaviour in the system.[48] It was argued that the momentum-reversal BMH method is analogous to a collisional process, effectively inducing randomisation in the system.[48] We had previously shown that each discontinuous jump in the modal momenta results in a randomisation of the vibrational phase,[27] and Peslherbe *et al.* have observed that the method effectively destroys the invariant tori which lead to quasiperiodic motion, by mapping trajectories in violation of ZPE constraints from these tori onto other invariant tori or chaotic regions of phase space.[24]

The motivations behind this paper are thus: To generalise the TRAPZ method to molecular systems of non-zero angular momentum. To test the TRAPZ method on RRKM and non-RRKM systems, in particular Al_3 dissociation and HNC isomerisation. The (RRKM *vs.* non-RRKM) effect of TRAPZ on a system of greater-than-two dimensions is investigated here.

In Section II, the TRAPZ method is generalised for use on molecular systems with non-zero angular momentum. The method is shown to involve the smallest perturbations to the Hamiltonian forces in order to preserve ZPE, conserve linear and angular momentum, and conserve total energy.

Details of calculations on Al_3 dissociation and HNC isomerisation are presented in Section III. Results and discussion are presented in Section IV. In Section IV we also show that TRAPZ does not conserve phase-space volume, which accounts in some way for chaotic → quasiperiodic behaviour.[27]

II. Theory

A. Notation

A derivation of the TRAPZ method has been published previously.[27] Here we present a derivation which acts on the instantaneous normal modes.[24,50] Henceforth, a single bar overscore is used to denote a vector of length $3N$, a double bar overscore a square matrix of linear dimension $3N$, and a tilde overscore a vector of length 3, where N is the number of atoms in the system. Hence the mass-weighted co-ordinates of atom i, $(x_{3i-2}, x_{3i-1}, x_{3i})$, are vectorially represented as

$$\tilde{x}_i = [x_{3i-2}\, x_{3i-1}\, x_{3i}]^T$$

We define mass-weighted coordinates and momenta, $(\bar{x}, \bar{p})$, in terms of the cartesian coordinates and momenta, $(\bar{x}_c, \bar{p}_c)$, as

$$\bar{x} = [x_1\, x_2 \cdots x_{3N}]^T$$

$$\bar{x} = \bar{\bar{M}}^{1/2}\bar{x}_c$$

and

$$\bar{p} = \bar{\bar{M}}^{-1/2}\bar{p}_c$$

where $\bar{\bar{M}}$ is the diagonal mass matrix

$$\bar{\bar{M}} = \mathrm{diag}[m_1\, m_1\, m_1\, m_2\, m_2\, m_2 \cdots m_N\, m_N\, m_N]$$

with m_i the mass of atom i.

B. The ZPE requirement

Firstly, consider the case of a non-rotating system, for which the total angular momentum, $\tilde{\boldsymbol{J}}$, is zero. We begin by taking the harmonic approximation to the potential energy surface at the instantaneous geometry, $\tilde{x}_t$:

$$V(\tilde{x}) \approx V(\tilde{x}_t) + \bar{f}(\tilde{x}_t)^T(\tilde{x} - \tilde{x}_t) + \tfrac{1}{2}(\tilde{x} - \tilde{x}_t)^T\bar{\bar{K}}(\tilde{x}_t)(\tilde{x} - \tilde{x}_t)$$

where

$$\bar{f}(\tilde{x}) = \left[\frac{\partial V(\tilde{x})}{\partial x_1}\ \frac{\partial V(\tilde{x})}{\partial x_2} \cdots \frac{\partial V(\tilde{x})}{\partial x_{3N}}\right]^T$$

and

$$\bar{\bar{K}}(\tilde{x}) = \begin{bmatrix} \frac{\partial^2 V(\tilde{x})}{\partial \tilde{x}_1^2} & \frac{\partial^2 V(\tilde{x})}{\partial x_1 \partial x_2} & \cdots & \frac{\partial^2 V(\tilde{x})}{\partial x_1 \partial x_{3N}} \\ \frac{\partial^2 V(\tilde{x})}{\partial x_2 \partial x_1} & \frac{\partial^2 V(\tilde{x})}{\partial x_2^2} & & \vdots \\ \vdots & & \ddots & \vdots \\ \frac{\partial^2 V(\tilde{x})}{\partial x_{3N} \partial x_1} & \cdots & \cdots & \frac{\partial^2 V(\tilde{x})}{\partial x_3^2 N} \end{bmatrix}$$

$\bar{\bar{K}}(\tilde{x})$ is the force constant matrix. We find the projected force constant matrix, $\bar{\bar{K}}_A(\tilde{x}_t)$, by removing the six infinitesimal rotations and translations from the matrix $\bar{\bar{K}}(\tilde{x}_t)$:[51]

$$\bar{\bar{K}}_A(\tilde{x}_t) = (\bar{\bar{I}} - \bar{\bar{A}}(\tilde{x}_t)\bar{\bar{K}}(\tilde{x}_t)(\bar{\bar{I}} - \bar{\bar{A}}(\tilde{x}_t)) \tag{3}$$

where $\bar{\bar{I}}$ is the identity matrix, and

$$\bar{\bar{A}}(\tilde{x}_t) = \begin{bmatrix} \sum_{i=1}^{6} A_{i,1}\, A_{i,1} & \sum_{i=1}^{6} A_{i,1} A_{i,2} & \cdots & \sum_{i=1}^{6} A_{i,1} A_{i,3N} \\ \sum_{i=1}^{6} A_{i,2}\, A_{i,1} & \sum_{i=1}^{6} A_{i,2} A_{i,2} & & \vdots \\ \vdots & & \ddots & \vdots \\ \sum_{i=1}^{6} A_{i,3N}\, A_{i,1} & \cdots & \cdots & \sum_{i=1}^{6} A_{i,3N} A_{i,3N} \end{bmatrix}$$

with $A_{i,j}$ the j-th component of the i-th unit vector for the infinitesimal rotations and translations of the molecule (six in all). Diagonalizing $\bar{\bar{K}}_A(\tilde{x}_t)$ we get the orthonormal eigenvectors $\bar{L}_k = [L_{k,1}\ L_{k,2} \cdots L_{k,3N}]^T$ corresponding to eigenvalues Ω_k^2 for $k = 1, \ldots, 3N$. These are the instantaneous normal modes.[50] $\bar{\bar{L}}$ is the matrix formed from the column vectors $\bar{L}_k$:

$$\bar{\bar{L}} = [\bar{L}_1\, \bar{L}_2 \cdots \bar{L}_{3N}]$$

The instantaneous normal mode coordinates and momenta, $(\bar{Q}, \bar{P})$, are related to the mass-weighted quantities by the equations

$$(\tilde{x} - \tilde{x}_t) = \bar{\bar{L}}\bar{Q}$$

and

$$\bar{p} = \bar{\bar{L}}\bar{P} \tag{4}$$

The Hamiltonian, expanded to second order in instantaneous normal mode coordinates, is

$$H(\bar{P}, \bar{Q}) = V(\tilde{x}_t) + \sum_{k=1}^{3N-6} (\tfrac{1}{2}P_k^2 + D_k Q_k + \tfrac{1}{2}\Omega_k^2 Q_k^2)$$

where the modes have been sorted: $1, \ldots, 3N-6$ are vibrational, and $3N-5, \ldots, 3N$ rotational and translational. The D_ks are given by

$$D_k = \bar{L}_k \cdot \bar{f}(\tilde{x}_t) \tag{5}$$

The second order expression for preservation of the zero-point energy in the vibrational normal modes is thence

$$\tfrac{1}{2}P_k^2 + \tfrac{1}{2}\Omega_k^2\left(Q_k + \frac{D_k}{\Omega_k^2}\right)^2 \geqslant \tfrac{1}{2}\hbar\Omega_k\,; \quad \text{for } k = 1, \ldots, 3N-6 \tag{6}$$

Note that $\frac{1}{2}\hbar\Omega_k$ is the instantaneous harmonic ZPE, given by the curvature of the potential surface in the neighbourhood of the instantaneous geometry $\tilde{x}_t$.

C. Non-rotating case ($J = 0$)

1. Preserving ZPE. Constraints[52,53] have been used to fix bond lengths in molecular dynamics simulations (*e.g.* ref. 54 and 55). Here constraints are used to fix certain mode energies at various times during a trajectory.

The TRAPZ method requires that whenever the system begins to violate eqn. (6), in one or more modes, those modes are constrained to the ZPE orbit, *i.e.*

$$\tfrac{1}{2}P_k^2 + \tfrac{1}{2}\Omega_k^2\left(Q_k + \frac{D_k}{\Omega_k^2}\right)^2 = \tfrac{1}{2}\hbar\Omega_k \qquad (7)$$

until there is energy redistribution back into these 'violating' modes,

$$\frac{\mathrm{d}}{\mathrm{d}t}\left[\tfrac{1}{2}P_k^2 + \tfrac{1}{2}\Omega_k^2\left(Q_k + \frac{D_k}{\Omega_k^2}\right)^2\right] > 0$$

when the trajectory is once again allowed to proceed unhindered (Fig. 1). Let the number of violating modes at any time be v, and assume the vibrational modes (*i.e.* 1, …, $3N - 6$) are re-sorted such that modes 1, …, v are violating. Neglecting the time dependences of $\bar{L}_k$ and Ω_k^2 differentiation of the constraint in eqn. (7), with respect to time, leads to

$$P_k\frac{\mathrm{d}P_k}{\mathrm{d}t} + \Omega_k^2\left(Q_k + \frac{D_k}{\Omega_k^2}\right)P_k = 0; \quad \text{for } k = 1, \ldots, v \qquad (8)$$

(Instantaneous normal mode bases depend on the molecular geometry which varies with time:[50] the final outcome is the same whether or not these variations of basis are included.) Combining eqn. (4) and (8), we arrive at the expression

$$\bar{L}_k \cdot \frac{\mathrm{d}\bar{p}}{\mathrm{d}t} = -\Omega_k^2\left(Q_k + \frac{D_k}{\Omega_k^2}\right); \quad \text{for } k = 1, \ldots, v$$

These v equations each represent a hyper-plane in $\mathrm{d}\tilde{p}/\mathrm{d}t$ (force) space, with normal vector $\bar{L}_k$. If the point representing the unconstrained force in $\mathrm{d}\bar{p}/\mathrm{d}t$ space does not lie on all of these hyper-planes, we map it to the nearest point which does, in order to preserve ZPE. This corresponds to the intersection

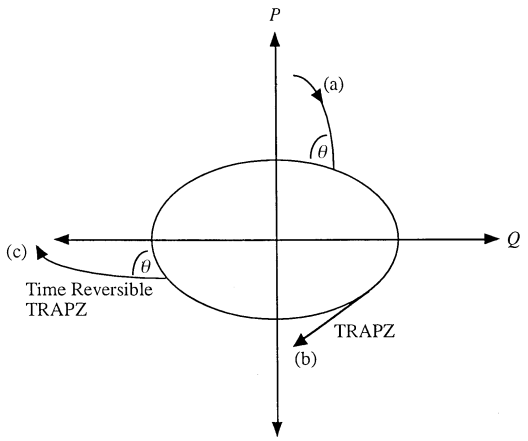

Fig. 1 Time-reversible and irreversible versions of TRAPZ. The diagram is for the phase space of a single vibrational mode, and represents a plot of momentum (P) *vs.* position (Q). A trajectory is seen moving in this space with time: (a) colliding with the ZPE orbit (ellipse), and eventually moving off the orbit either (b) tangentially (time-irreversible case),[27] or (c) at an angle equal to that at which it approached the orbit (time-reversible case).[43]

of another hyper-space (which passes through the unconstrained point and is spanned by the $\bar{L}_k$ vectors), with the v constraint hyper-planes. For example, if there is only one violating mode, the point is moved in the $\bar{L}_k$ (normal) direction until it satisfies eqn. (7). Obviously, following the normal vector corresponds to the shortest distance between a point and a plane. The equation of motion for $\mathrm{d}\bar{p}/\mathrm{d}t$ is now

$$\frac{\mathrm{d}\bar{p}}{\mathrm{d}t} = -\frac{\partial V(\tilde{x})}{\partial\tilde{x}} + \sum_{k=1}^{v}\lambda_k\bar{L}_k$$

The equation for $\mathrm{d}\tilde{x}/\mathrm{d}t$ is unchanged. [This is slightly different from our original prescription which used a radial mapping in (P_k, Q_k) space.][27] The λ_k coefficients

$$\lambda_k = \lambda_k(P_k, Q_k)$$

for each violating normal mode, are chosen so as to ensure preservation of ZPE in mode k. A better representation is obtained by transforming to normal mode coordinates, which gives

$$\frac{\mathrm{d}P_k}{\mathrm{d}t} = -\frac{\partial V(\bar{Q})}{\partial Q_k} + \lambda_k; \quad \text{for } k = 1, \ldots, v$$

$$\frac{\mathrm{d}Q_k}{\mathrm{d}t} = P_k; \quad \text{for } k = 1, \ldots, v \qquad (9)$$

Each λ_k can be determined by solving eqn. (8) and (9) simultaneously. Changes to the equations for the non-violating modes are considered next.

2. Conservation of total energy. The conservation of total energy gives an extra constraint,

$$\frac{\mathrm{d}H(\bar{P}, \bar{Q})}{\mathrm{d}t} = \sum_{k=1}^{3N-6}\left(P_k\frac{\mathrm{d}P_k}{\mathrm{d}t} + \frac{\partial V(\bar{Q})}{\partial Q_k}P_k\right) = 0 \qquad (10)$$

Transformation of parts of eqn. (10) to mass-weighted coordinates gives

$$\left[\sum_{k=1}^{3N-6}P_k\bar{L}_k\right]\cdot\frac{\mathrm{d}\bar{p}}{\mathrm{d}t} = -\sum_{k=1}^{3N-6}\frac{\partial V(\bar{Q})}{\partial Q_k}P_k \qquad (11)$$

This is another hyper-plane in $\mathrm{d}\bar{p}/\mathrm{d}t$ space, with the normal vector

$$\sum_{k=1}^{3N-6}P_k\bar{L}_k \qquad (12)$$

However, this normal is not guaranteed to be orthogonal to the $\bar{L}_k$ normal vectors which arose from preserving ZPE. We wish to add this vector to the ZPE constraint normals found previously, thus forming a new space, spanned by $v + 1$ vectors, which passes through the unconstrained point in $\mathrm{d}\bar{p}/\mathrm{d}t$ space. We can establish an orthogonal basis for this space by simply excluding the 1, …, v terms from the summation on the left-hand side of eqn. (12). This new space will intersect all of the ZPE constraint hyper-planes, and that expressed by eqn. (11), at a single point. A physical interpretation of mapping to this point is that it represents the smallest possible change to the force on the molecule which leads to preservation of zero-point energy and conservation of total energy. The equations of motion for the non-violating modes thus become

$$\frac{\mathrm{d}P_k}{\mathrm{d}t} = -\frac{\partial V(\bar{Q})}{\partial Q_k} + \beta P_k; \quad \text{for } k = v + 1, \ldots, 3N - 6$$

$$\frac{\mathrm{d}Q_k}{\mathrm{d}t} = P_k; \quad \text{for } k = v + 1, \ldots, 3_{N-6} \qquad (13)$$

$\beta = \beta(\bar{P}, \bar{Q})$ is chosen to ensure conservation of total energy and is determined by solving eqn. (8), (9), (10), and (13).

D. Implementation by numerical integrator

2. The complete mapping. The above equations of motion are integrated by a numerical algorithm. Hence, the time rate of change of non-violating normal mode momentum, in differential form,

$$\delta P_k = -\frac{\partial V(\tilde{Q})}{\partial Q_k}\,\delta t + \beta P_k\,\delta t; \quad k = v+1, \ldots, 3N-6$$

is discretised as

$$\begin{aligned}\Delta P_k &= -\left[\frac{\partial V(\bar{Q})}{\partial Q_k} + O(\Delta t)\right]\Delta t + [\beta P_k + O(\Delta t)]\Delta t \\ &\cong -\left[\frac{\partial V(\tilde{Q})}{\partial Q_k} + O(\Delta t)\right]\Delta t + \beta P_k \Delta t \end{aligned} \tag{14}$$

for a small time step, Δt, and change in momentum, ΔP_k. The right-hand side of eqn. (14) comprises two terms: the usual Hamiltonian force expansion, with a TRAPZ correction using the method of undetermined coefficients.[52,53] The discrete equations for the violating modes have the same form:

$$\Delta P_k \simeq -\left[\frac{\partial V(\bar{Q})}{\partial Q_k} + O(\Delta t)\right]\Delta t + \lambda_k \Delta t; \quad \text{for } k = 1, \ldots, v \tag{15}$$

The equations for ΔQ_k are the same as for the unconstrained (classical) system:

$$\Delta Q_k \simeq [P_k + O(\Delta t)]\Delta t \tag{16}$$

In applying TRAPZ to a numerically integrated system with discrete time steps, we simply modify the vibrational-normal-mode momenta at the completion of each time step. For the violating modes, this involves mapping the unconstrained momentum $P_k \rightarrow P'_k$, where P'_k is found by inverting eqn. (7) and is

$$P'_k = \text{sign}(P_k)\sqrt{\hbar\Omega_k - \frac{D_k^2}{\Omega_k^2}}; \quad \text{for } k = 1, \ldots, v \tag{17}$$

We map all the non-violating mode momenta by a constant factor, β':

$$P'_k = \beta' P_k; \quad \text{for } k = v+1, \ldots, 3N-6 \tag{18}$$

This is not the exact mapping prescribed by eqn. (14), since the P_k used in this expression is the unconstrained momentum of mode k *after* a time step, *not before* the time step. The difference is generally negligible (and exact in the limit as $\Delta t \rightarrow 0$): making this approximation leads to a simpler formulation. We require that the TRAPZ correction in eqn. (17) and (18) conserves total energy

$$\begin{aligned}\tfrac{1}{2}\sum_{k=1}^{3N-6} P_k^2 + V &= \tfrac{1}{2}\sum_{k=1}^{3N-6} P_k'^2 + V \\ &= \tfrac{1}{2}\sum_{k=1}^{v} P_k'^2 + \tfrac{1}{2}(\beta')^2 \sum_{k=v+1}^{3N-6} P_k^2 + V\end{aligned}$$

Note the potential energy term, V, is not affected by the TRAPZ mapping [eqn. (17) and (18)]. Solving for β' gives

$$\begin{aligned}\beta' &= \sqrt{1 - \frac{\sum_{k=1}^{v} P_k'^2 - P_k^2}{\sum_{k=v+1}^{3N-6} P_k^2}} \\ &= \left(\frac{\sum_{k=1}^{3N-6} P_k^2 - \sum_{k=1}^{v} P_k'^2}{\sum_{k=v+1}^{3N-6} P_k^2}\right)^{1/2}\end{aligned} \tag{19}$$

with the restriction that

$$\sum_{k=1}^{v} P_k'^2 \leqslant \sum_{k=1}^{3N-6} P_k^2 \tag{20}$$

so that β' is a real quantity.

2. The incomplete mapping. Eqn. (20) states that kinetic energy from the non-violating modes is redistributed into the violating modes in order to preserve ZPE. For systems with a small number of oscillators, there is a small but significant probability that all the non-violating modes have a small amount of kinetic energy which *might* not satisfy eqn. (20). In this event, ZPE preservation is sacrificed to ensure conservation of energy. The rare occurrence of this requires a (un)fortuitious matching of the vibrational phases of all the non-violating modes and is less likely the larger the number of modes. At the same time, as much energy is shifted from the non-violating modes into the violating modes as possible. This is achieved as follows:

$$P'_k = 0; \quad \text{for } k = v+1, \ldots, 3N-6 \tag{21}$$

$$P'_k = \gamma P_k; \quad \text{for } k = 1, \ldots, v \tag{22}$$

$$\gamma = \sqrt{\frac{\sum_{k=1}^{3N-6} P_k^2}{\sum_{k=1}^{v} P_k^2}} \tag{23}$$

E. Non-zero angular momentum

1. Orthogonality of vibrational and rotational/translational modes. The above formulation of TRAPZ makes no explicit attempt to conserve linear or angular momentum. This is unnecessary, because the instantaneous normal vibrational modes are orthogonal to the rotational and translational modes of the system. [The rotational and translational modes have been projected out of the force constant matrix: eqn. (3).] This assures that any change to vibrational mode momenta will have no effect on the total linear or angular momentum (apart from numerical error in the diagonalisation routine.) These orthogonality conditions are often referred to as the Eckart conditions or Sayvetz conditions.[56,57] The Sayvetz conditions for a rotating molecule can be written as

$$\sum_{i=1}^{N} m_i(\tilde{r}_i - \tilde{r}_i^t) = \tilde{0}$$

$$\sum_{i=1}^{N} m_i \tilde{r}_i^t \times \frac{\mathrm{d}\tilde{r}_i}{\mathrm{d}t} = \tilde{0}$$

where $\tilde{r}_i^t$ is the instantaneous non-mass-weighted position vector of atom i with respect to the *molecule-fixed* frame. By simply aligning the molecule and space-fixed axes,

$$\sum_{i=1}^{N} \sqrt{m_i}\,\tilde{L}_{i,k} = \tilde{0} \tag{24}$$

$$\sum_{i=1}^{N} \tilde{x}_i \times \tilde{L}_{i,k} = \tilde{0} \tag{25}$$

The change in linear and angular momentum, $\Delta\tilde{p}_{\text{tot}}$ and $\Delta\tilde{J}$, respectively, induced by a shift in the momenta of each of the vibrational normal modes, ΔP_k for $k = 1, \ldots, 3N-6$, can be expressed as[24]

$$\Delta\tilde{p}_{\text{tot}} = \sum_{k=1}^{3N-6}\sum_{i=1}^{N} \Delta P_k \sqrt{m_i}\,\tilde{L}_{i,k} \tag{26}$$

$$\Delta\tilde{J} = \sum_{k=1}^{3N-6}\sum_{i=1}^{N} \Delta P_k(\tilde{x}_i \times \tilde{L}_{i,k}) \tag{27}$$

Eqn. (26) and (27) are equal to zero due to eqn. (24) and (25) and, therefore, no change to the momenta of the instantaneous normal vibrational modes can have any effect on the total linear and angular momentum of the system (apart from numerical error).[24]

In practice, it is important to check the Sayvetz conditions at each time step, to minimise numerical error. For this reason, whenever the norm of the left-hand side of eqn. (24) and (25) are greater than an arbitrary tolerance,

$$\left| \sum_{i=1}^{N} \sqrt{m_i} \tilde{L}_{i,k} \right| > TOL$$

mode k is treated as a translational mode, whilst if

$$\left| \sum_{i=1}^{N} \tilde{x}_i \times \tilde{L}_{i,k} \right| > TOL$$

mode k is regarded as a rotation. This is the case even if other measures, such as relative size of eigenvalues, suggest that the mode is vibrational.

2. TRAPZ for systems of non-zero angular momentum. The only aspect of the above TRAPZ algorithm (sub-Sections II A–II D) which needs to be reformulated for rotating systems is the calculation of normal mode momenta, purely to reduce numerical error. For rotating systems, we simply replace eqn. (4) with

$$P_k = \sum_{i=1}^{N} \tilde{L}_{i,k} \cdot [\tilde{p}_i - (\tilde{\omega} \times \tilde{x}_i)] \quad (28)$$

where $\tilde{\omega}$ is the angular velocity, in order to transform from mass-weighted to normal mode momenta. The inverse transformation,

$$\tilde{p}_i = (\tilde{\omega} \times \tilde{x}_i) + \sum_{k=1}^{3N-6} P_k \tilde{L}_i, \quad (29)$$

is used to determine the mass-weighted momenta from the normal mode values.

F. Computational algorithm

The TRAPZ process, for use with instantaneous normal modes, can be summarised by the following algorithm:

1. Integrate Hamilton's equations one time step in cartesian coordinates.

2. Evaluate and diagonalise the projected force constant matrix [eqn. (3)] to get the instantaneous normal modes.[50] Check the Sayvetz conditions [eqn. (24) and (25)] for each mode to determine which can be treated as vibrational.

3. Determine P_k [eqn. (4) or (28)] and D_k [eqn. (5)] for the vibrational modes and, hence, find the mode energies and instantaneous harmonic ZPEs. Establish which modes are in violation of harmonic ZPE constraints [eqn. (6)].

4. Test if a full mapping is possible using eqn. (20).

(a) If so: determine β' and map all mode momenta according to eqn. (14)–(18), (19), and (20).

(b) Otherwise: establish γ and map the violating and non-violating modes according to eqn. (21)–(23).

5. Transform the constrained normal mode momenta into mass-weighted and hence cartesian forms [eqn. (4) or (29)].

6. Repeat from step 1.

III. Details of calculations

A. Potential-energy surfaces

1. Al_3 dissociation. The Al_3 potential-energy surface used in this study is the same as that utilised by Peslherbe *et al.*[44,45] It consists of two-body Lennard-Jones potential functions, and a three-body Axilrod–Teller function,[58–61] both of which are standard options in the dynamics program VENUS96.[62] Standard numerical routines were utilised for the spatial second derivatives of the potential-energy surface.

A contour plot of the surface is shown in Fig. 2, for $J = 0$, with one bond length fixed at the global minimum value of 0.2712 nm. The classical dissociation limit lies 36.97 and 30.82 kcal mol^{-1} (154.7 and 129.0 kJ mol^{-1}) above the global (triangular) and secondary (linear) minima respectively.[44] It is necessary to sample[62,63] trajectory initial conditions around both minima.

2. HNC isomerisation. The HNC potential-energy surface was that used by Shen *et al.*,[48,49] and originally due to Murrell *et al.*[64] A contour plot with the N—C bond length fixed at the equilibrium HNC value of 0.116 nm is shown in Fig. 3. It depicts two minima, both linear, for the HNC reactant and for the HCN product, separated by a barrier of 23.6 kcal mol^{-1} (98.7 kJ mol^{-1}).

B. Selection of initial conditions

Initial conditions were selected using microcanonical normal mode sampling, which is exact for harmonic oscillators.[63] Only systems for which $J = 0$ were tested, although the method is equally applicable to rotating cases. Since the TRAPZ microcanonical ensemble is a subset of the classical microcanonical ensemble,[31] the TRAPZ ensemble was obtained from the classical ensemble by "rejecting" non-TRAPZ initial conditions (*i.e.* those that violated the ZPE conditions [eqn. (6)]).

1. Al_3 dissociation. Microcanonical ensembles with energies between 3 and 13 kJ mol^{-1} above the classical threshold were used. The quantum reaction threshold (the vibrational ZPE of an isolated Al_2 dimer) is *ca.* 2.9 kJ mol^{-1}above the classical threshold. Following the approach of Peslherbe and Hase, approximately half of the trajectories were started from each configuration (linear and triangular).[44] At a total energy of 8.4 kJ mol^{-1}, the TRAPZ ensemble subsets were 89% (triangular configuration) and 97% (linear) of the equivalent classical ensembles.

2. HNC isomerisation. All the HNC trajectories had a total energy of 2.5 eV (241 kJ mol^{-1}). At this energy, the TRAPZ ensemble subset was 87% of the equivalent classical ensemble.

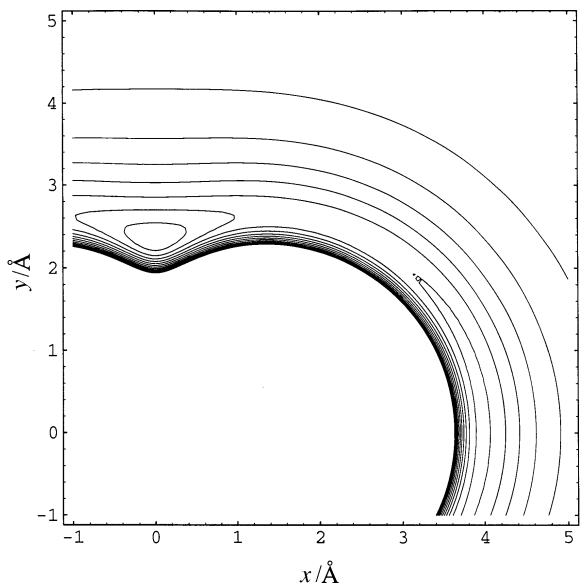

Fig. 2 Contour plot of the $J = 0$ potential-energy surface of Al_3 used in this study. Two atoms are symmetrically placed on the x-axis at $x = \pm 1.356$ Å. The potential energy is then plotted against the position of the third atom in the (x, y) plane. Contour energies vary by 5 kcal mol^{-1} from one line to the next. The plot shows two minima, one when the atoms form an equilibrium triangle, and another which is for a linear configuration.

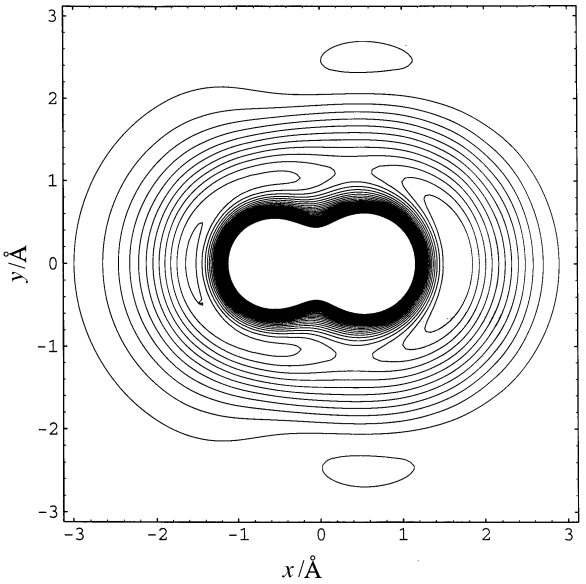

Fig. 3 Contour plot of the $J = 0$ potential energy surface of HNC used in this study. The N and C atoms are symmetrically placed on the x-axis about $x = 0$ (N to the left and C to the right) with separation fixed at the HNC equilibrium C—N bond length of 1.16 Å. The potential energy is plotted against the position of the H atom in the (x, y) plane. Contour energies vary by *ca.* 10 kcal mol^{-1} from one line to the next. The plot shows two minima, one for HNC and the other for HCN, as well as clearly defined barriers of isomerisation.

C. Analysis of data

In order to determine rate coefficients, the time at which reactant Al_3 becomes product Al_2 + Al needs to be defined. There are at *least two* possible criteria for this lifetime (or time of evaporation) of the cluster:

The time from the start of the trajectory until the kinetic energy of the evaporating monomer stops fluctuating and begins to decrease monotonically. This standard criterion was utilised in *unconstrained* classical trajectory calculations of the dissociation of Al_3 by Peslherbe *et al.*[44] but active constraints can lead to fluctuations in momenta which make this method unsuitable.[45]

The time from the start of the trajectory until the last turning point in the relative velocity of the evaporating monomer to the centre of mass of the product dimer. This criterion has been used by Peslherbe *et al.* for their work with constrained Al_3,[45] and is the criterion employed in this study.

These two criteria can lead to quite different results for any one trajectory: the lifetime is generally shorter when calculated by the relative velocity technique, as opposed to the oscillating kinetic energy method.

For HNC, the criterion for reaction was when the line joining the C—N centre of mass to the H atom, made an angle with the C—N line of centres, that was greater than or equal to 113.1°.[49] Calculations for HNC exhibit a rapid initial reaction ($t \lesssim$ *ca.* 100 fs: two bending vibrational periods), which is attributed to 'direct' trajectories.[49] The selection of initial conditions is such that some trajectories are initiated *in the transition state region.* These trajectories pass directly to form products in a few vibrational periods and are removed from any rate analysis.

Rate coefficients k_1 and k_2 are determined from either a single- or double-exponential decay of the number of unreacted trajectories

$$N(t) = N(0)[ce^{-k_1 t} + (1 - c)e^{-k_2 t}]$$

D. Classical and TRAPZ calculations

Classical trajectory calculations were also performed for comparison. This was particularly critical since direct comparison with the classical-trajectory results of other authors[44,45] is not possible due to the differences in criteria for trajectory lifetime discussed in sub-Section III C. Generally, less trajectories were run for the TRAPZ method, due to the extra computation required. TRAPZ trajectories were found to require ten times the computer time for (unconstrained) classical trajectories of an equal number of timesteps. This is due to the instantaneous normal-mode analyses which are performed at every timestep. In addition, TRAPZ trajectories dissociated more slowly, particularly at energies close to quantum dissociation threshold.

E. Method of integration

TRAPZ simulations were performed with the dynamics program VENUS96,[62] modified to implement the TRAPZ method, using a fourth-order Runge–Kutta–Gill routine. Classical simulations were performed with an unmodified version of VENUS96,[62] using a sixth-order Adams–Moulton predictor-corrector method after initiation by the fourth-order Runge–Kutta–Gill routine. The step size for all Al_3 simulations was chosen to be 0.1 fs, which was found to conserve energy to better than 4×10^{-4} kJ mol^{-1} over the length of a trajectory. For HNC, a step size of 0.01 fs assured energy conservation to better than 4×10^{-6} kJ mol^{-1}.

IV. Results and discussion

A. RRKM *vs.* non-RRKM behaviour

TRAPZ Al_3 trajectories were found to have single-exponential decay. This indicates that the TRAPZ method has preserved the intrinsic RRKM nature of the system.

Classical HNC calculations by Chan *et al.*[49] and in this work show non-RRKM biexponential decay. In contrast, the TRAPZ calculations (Table 1) show RRKM-like single-exponential decay. As the constraint energy is varied

$$\tfrac{1}{2}P_k^2 + \tfrac{1}{2}\Omega_k^2 Q_k^2 \geqslant \tfrac{1}{2}\kappa\hbar\Omega_k \qquad (30)$$

from $\kappa = 0$ (classical) to $\kappa = 1$ (TRAPZ) there is a gradual transition from biexponential to single-exponential decay. The four sets of results in Table 1 differ in the choice of the parameter κ [eqn. (30)]: switching from classical trajectories [$\kappa = 0$: case (a)], through intermediate cases [$\kappa = 0.1$ and 0.5: (b) and (c), respectively], to the TRAPZ procedure [$\kappa = 1$: case (d)].

$\kappa = 0$. Rate constants k_1 and k_2 differ by one-and-a-half orders of magnitude (Table 1). The two exponential terms each contribute about half ($c = 0.48$) of the decay.

$\kappa = 0.1$ and $\kappa = 0.5$. These intermediate cases show that the slow-decay term has become faster: k_1 and k_2 differ by approximately half an order of magnitude (Table 1) and that the contribution from the first (faster-)decay term has increased from approximately half to almost unity ($c = 0.92$).

Table 1 Biexponential fits for the TRAPZ isomerisation of HNC with various constraint factors (κ)

κ	c	$k_1/10^9$ s^{-1}	$k_2/10^9$ s^{-1}	k_2/k_1
0.0	0.48	4.39	0.086	0.02
0.1	0.54	2.09	0.667	0.3
0.5	0.92	2.82	0.489	0.2
1.0	1[a]	2.47	—	—

[a] Single exponential fit.

$\kappa = 1$. Single-exponential decay, indicates RRKM (or ergodic) behaviour. Statistical analysis indicates that there is no evidence for a double-exponential decay (>99.99% confidence level).

Chaotic behaviour (which is one type of ergodic behaviour) is *possible* for coupled non-linear differential equations of three or more (otherwise) independent variables. The TRAPZ algorithm represents an additional time- and vibrational-basis-dependent (*i.e.* non-linear) coupling of the usual Hamilton's equations of motion. Thus TRAPZ has the *potential* for ergodicity, even in the otherwise[49] non-RRKM (*i.e.* non-ergodic) HNC system. Hence, the observed ergodicity is not surprising. Another way of thinking about this behaviour is that TRAPZ destroys most of the invariant tori which lead to quasiperiodicity.

In some earlier studies, we found that a slightly different implementation of TRAPZ led to quasiperiodic limit-cycle behaviour in the otherwise chaotic Hénon–Heiles system.[27,33,34] In that particular implementation, the projection of the violating mode (Q_k, P_k) onto the ZPE orbit [eqn. (6)] reduced the total phase-space volume available to the system. This is discussed below.

B. Al_3 dissociation rate coefficients

1. Rate coefficients. Rate coefficients for TRAPZ and classical calculations are presented in Table 2 and Fig. 4. The classical-trajectory rate coefficients vary somewhat from those found by Peslherbe *et al.*,[44] due to the statistical uncertainties inherent in a small ensemble, and the different criteria used to determine trajectory lifetime. Our results do not support the conclusions of Peslherbe *et al.* that the rates for an ensemble initiated about the linear minimum tend to be greater than for the corresponding triangular quantities at all energies.[44]

2. Comparison with quantum RRKM rates. RRKM rate coefficients have been calculated using quantum anharmonic flexible transition-state theory,[65–68] following the implementation of Peslherbe *et al.*[45] (see Table 2 and Fig. 4). The slope discontinuity in the RRKM results at *ca.* 9.5 kJ mol^{-1} above the classical dissociation limit corresponds to the threshold for excited Al_2 product in the first vibrational overtone state. *Quantum RRKM rates are an upper bound to the true (quantum) rate*[61,69] and, hence, are used here as an *absolute* standard against which trajectory results can be compared. (Note that there can be no quantum tunnelling in a barrierless reaction.)

As expected, the classical trajectory rate coefficients in an ergodic (*i.e.* RRKM) system approximate or exceed the RRKM rates at all energies. The classical trajectory rate coefficients exceed the RRKM ones in two energy regimes: near and below the thresholds for reaction and for formation of excited Al_2 product.

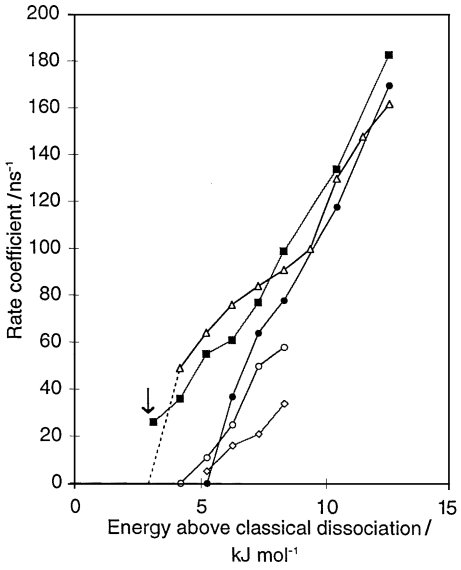

Fig. 4 Al_3 dissociation rate coefficients (10^9 s^{-1}) *vs.* energy E_{ex} above classical dissociation limit: classical trajectory method (■); TRAPZ method (●); TRAPZ-(κ_{WR}) method (○); BMH method (◇) taken from ref.;[45] and quantum-anharmonic flexible-transition-state RRKM theory (△).

The TRAPZ and BMH rate coefficients are less than the RRKM limit for energies up to *ca.* 11 kJ mol^{-1} above the classical dissociation limit. Both these methods have prevented the formation of product dimers with less than vibrational ZPE.

There is good agreement between the different methods at energies above *ca.* 11 kJ mol^{-1} above the classical dissociation limit. We suggest that this is a crude manifestation of the quantum-classical correspondence principle which is observed at high(er) energies. (The minor discrepancies between the different rate cofficients in this energy regime are most probably due to the trajectory transition states being slightly different from the variational RRKM transition state which occurs at larger separations than the trajectory ones.)

3. Reaction threshold. *The BMH and TRAPZ rate coefficients are zero at some energies higher than the asymptotic constraint threshold of 0.7 kcal mol^{-1} (2.9 kJ mol^{-1}) above the classical dissociation limit* (indicated by the arrow in Fig. 4). This effect is due to variations in instantaneous normal mode bases, which raises the apparent ZPE, reducing the energy available to the reaction coordinate and hence lowering the rate coefficient. Fig. 5 depicts a typical example of this behaviour for a single dissociating TRAPZ trajectory.

Fig. 5(a) shows the energy of the conserved instantaneous-normal mode, which asymptotically becomes the dimer vibration, *versus* dimer-monomer centre of mass separation. Fig.

Table 2 Trajectory rate coefficients for $Al_3 \rightarrow Al_2 + Al$[a]

E_{ex}[b]		Classical			TRAPZ			BMH	RRKM
kcal/mol^{-1}	kJ/mol^{-1}	k_{tri}[c,e]	k_{lin}[c,f]	k_{ave}[g]	k_{tri}[d,e]	k_{lin}[d,f]	k_{ave}[g]	k_{traj}[h]	k_{RRKM}[i]
0.75	3.14	25	25	26					
1.00	4.18	34	38	36					49
1.25	5.23	53	54	55	<1	<1	<1	5	64
1.50	6.28	63	61	61	46	29	37	16	76
1.75	7.32	73	74	77	69	72	64	21	84
2.00	8.37	92	100	99	78[c]	81[c]	78	34	91
2.50	10.46	131[j]	139[j]	134	118[j]	115[j]	117		130
3.00	12.55	180[j]	187[j]	183	167[j]	175[j]	170		162

[a] All rate coefficients are in 10^9 s^{-1}. [b] Energy in excess of classical dissociation threshold. [c] Ensembles of 200 trajectories. [d] Rate coefficients are for 100 trajectories, unless specified otherwise. [e] Sampled around the triangular geometry. [f] Sampled around the linear geometry. [g] Average of rates for the triangular and linear geometries. [h] Trajectory calculated rate coefficients from reference for the BMH method. [i] Quantum anharmonic flexible transition-state theory. [j] Ensembles of 500 trajectories.

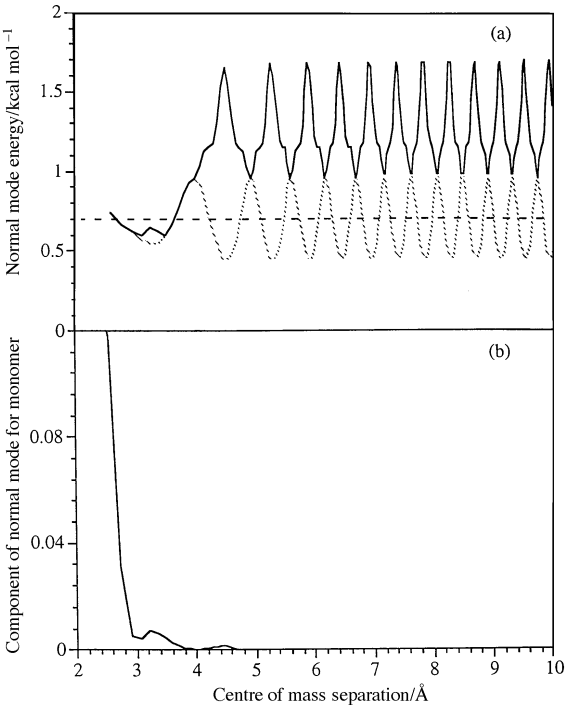

Fig. 5 Behaviour of the Al_3 instantaneous normal mode which asymptotically represents the product dimer vibration. (a) Instantaneous mode energy (———) and ZPE (.....) *vs.* separation of dimer centre of mass and evaporating atom, for a single trajectory 2.0 kcal mol^{-1} above classical threshold. The dashed horizontal line represents the actual product dimer ZPE. (b) Norm of the mode component that pertains to the evaporating atom, also *vs.* centre of mass separation.

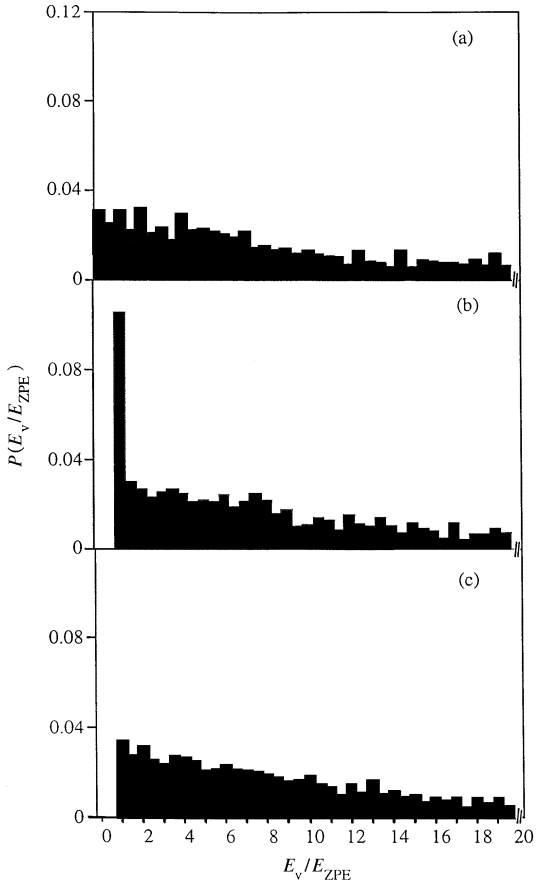

Fig. 6 Histogram plot of the probability that any vibrational instantaneous normal mode, will have a particular ratio of mode energy to ZPE (E_v/E_{ZPE}). The plots are for a non-dissociating Al_3 trajectory of length 10 ps and energy 30 kcal mol^{-1} above the global minimum. The horizontal axes have been truncated at $E_v/E_{ZPE} = 20$, since the behaviour of interest occurs around the ZPE ($E_v/E_{ZPE} = 1$). (a) classical system; (b) TRAPZ method; and (c) BMH method.

5(b) is the norm of the component of this mode that pertains to the evaporating monomer. From Fig. 5(b) it is clear that the monomer component quickly drops to zero, meaning that the instantaneous-normal mode effectively represents the dimer vibration at separations greater than *ca.* 0.4 nm. In Fig. 5(a), it can be seen that the mode energy is forced higher by the constraint at around 0.35 nm and then is relatively unaffected by the constraint for the rest of the trajectory. After this initial interaction, the energy is seen to oscillate quasi-periodically, along with the instantaneous ZPE [eqn. (6)], for the rest of the evaporation. This oscillation is due to time variation of the instantaneous normal mode basis. The instantaneous mode energy is seen to oscillate about the product dimer energy of 1.15 kcal mol^{-1} (4.8 kJ mol^{-1}), and the instantaneous ZPE oscillates about the isolated dimer ZPE of 0.7 kcal mol^{-1} (2.9 kJ mol^{-1}). The net result is to increase the 'effective' constraint energy to greater than dimer ZPE.

4. Comparison between TRAPZ and BMH rate coefficients. *The TRAPZ rate coefficients are significantly larger than those predicted by the BMH method.* Fig. 6 shows the time-averaged distribution of *reactant* vibrational mode energies, as a fraction of ZPE, for classical (a), TRAPZ (b) and BMH (c) trajectories, all at the same energy *below* the classical dissociation threshold. The horizontal axes have been truncated, since the interesting behaviour occurs around the ZPE. The TRAPZ method, as expected, forbids any E_v/E_{ZPE} values less than unity. However, more importantly, it does not redistribute those excluded 'probabilities' over the whole range of mode energies, as is the case for the BMH method. Instead, the density of mode energies is concentrated around the ZPE value.

Hence, in a dissociating BMH trajectory, the vibrational modes orthogonal to the reaction coordinate are more likely to be at higher vibrational energy than in the TRAPZ case, and the reaction coordinate will correspondingly have less energy available to it, decreasing the BMH rates relative to the equivalent classical-trajectory, RRKM and TRAPZ rate coefficients.

C. Al_3 product distributions

1. Vibrational energy distributions. Product Al_2 vibrational energy distributions are shown in Fig. 7 for TRAPZ and classical ensembles, at $E_{ex} = 8.4$ kJ mol^{-1} above classical asymptotic limit. The classical trajectories have a broad distribution, with population below product ZPE, and a tail to higher energy [Fig. 7(a)], consistent with a (classical-mechanics) statistical distribution.

The TRAPZ vibrational energy distribution [Fig. 7(c)] has a threshold or lower bound significantly above the true ZPE threshold. Interestingly, a large spike occurs at this lower bound (which could be considered the 'effective' constraint energy). This entrainment of dimer vibrational energy, by the TRAPZ method, is the effect alluded to earlier. The Al_2 dimer vibrational energy is forced to increase, as the corresponding normal mode follows the instantaneous harmonic ZPE orbit near the beginning of monomer evaporation and, thereafter, is relatively constant. It seems that this process is very similar in each case: TRAPZ forces most trajectories into a similar energetic configuration at this critical point of the evaporation. For a different method, such as BMH, the mode energy does not follow the ZPE for any length of time and this standardisation will not occur.

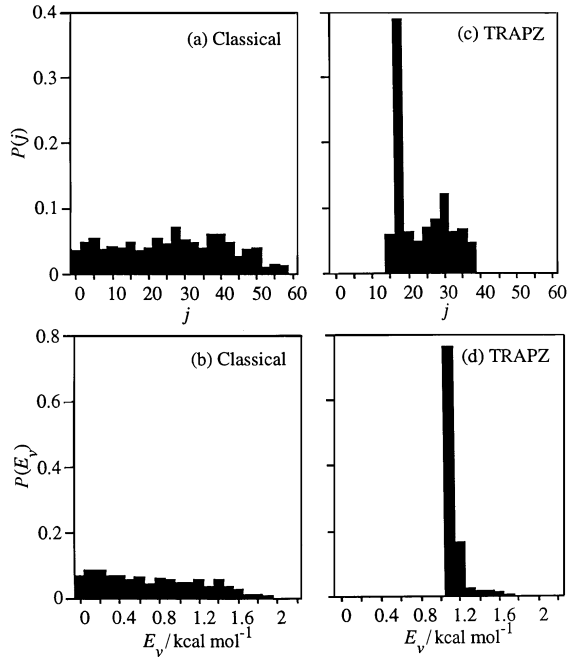

Fig. 7 Product dimer probability distributions. (a) Angular momentum ($\hbar$ units) distribution for an unconstrained classical ensemble at an energy of 2.0 kcal mol^{-1} above classical threshold. (b) Vibrational energy distribution for the same ensemble; (c) and (d) analogous angular momentum and vibrational energy distributions for the equivalent TRAPZ ensemble. Each ensemble is 400 trajectories in size, with approximately half initiated around each equilibrium configuration.

2. Angular momentum distribution. Product Al_2 angular momentum distributions are also shown in Fig. 7. Note the non-zero threshold in the TRAPZ simulations [Fig. 7(d)]. The reactant bending mode must initially have at least ZPE, which is then converted into product dimer rotation upon dissociation. This effect could be the result of TRAPZ overconstraining the reactant molecules, resulting in excessive bending mode energy. This is supported by the higher than expected TRAPZ reaction threshold, which suggests too much energy is also being channelled into the dimer vibration early in the evaporation process [Fig. 7(c)]. An improved method could involve reducing the potency of the constraint on reactant molecules, and increasing its effect for molecules in the transition state region.

3. Lowering the constraint energy. The product distributions imply that the instantaneous harmonic ZPE, $\hbar\Omega_k/2$, may be a too-severe constraint energy in many instances. Other authors have come to similar conclusions.[28,33,45,70] The scaling parameter κ [eqn. (30)] enables the forbidden region to be scaled without altering the fundamental nature of the TRAPZ method. For the Al_3 system, some TRAPZ trajectories were performed where κ was varied *at each time step* according to the Whitten–Rabinovitch formulation:[71,72]

$$\kappa_{\mathbf{WR}} = \beta w\left(\frac{2E}{\hbar\Omega_k}\right)$$

where β and w are the Whitten–Rabinovitch parameters,[71,72] calculated by finding the total instantaneous-normal-mode vibrational energies and instantaneous harmonic ZPE. This variant of TRAPZ is denoted "TRAPZ-($\kappa_{\mathbf{WR}}$)".

TRAPZ-($\kappa_{\mathbf{WR}}$) rate coefficients are shown in Fig. 4, for ensembles of trajectories initiated in the linear configuration. At high energies, the rate coefficients are lower than the standard TRAPZ results, but are higher at low energies. The effective constraint threshold is less (*i.e.* approximately $E_{\mathbf{ex}} = 4.2$ kJ mol^{-1}). Importantly, the TRAPZ-($\kappa_{\mathbf{WR}}$) rate coefficients are less than the quantum RRKM estimates at all energies tested.

The lowering of the effective constraint energy, brought about by introducing $\kappa_{\mathbf{WR}}$, is a result of the lower bound on product dimer angular momenta having been eliminated (Fig. 8). Whereas, in Fig. 7, the TRAPZ angular momentum distribution has a clear lower limit in the range $j = 10\hbar - 15\hbar$, Fig. 8(a) displays values of j right down to zero. Some of the energy which was previously trapped in the Al_2 rotation, is thus accessible to the reaction coordinate, which allows trajectories to dissociate at lower total energies. Note too, that the TRAPZ-($\kappa_{\mathbf{WR}}$) Al_2 vibrational energy distribution [Fig. 8(b)] includes a greater proportion of trajectories at higher energies *i.e.* 1.5–2.0 kcal mol^{-1} (6.3–8.4 kJ mol^{-1}). This also is the result of extra energy being made available by the removal of the lower bound on j.

The TRAPZ-($\kappa_{\mathbf{WR}}$) vibrational energy plot [Fig. 8(b)] is not as peaked as it was for the standard TRAPZ method. A peak does exist at the lower bound, but it is broader and shorter. Interestingly, the lower bound itself is unchanged. Clearly the TRAPZ-($\kappa_{\mathbf{WR}}$) does not entrain trajectories to the same degree as standard TRAPZ , but the increase in effective reaction threshold caused by oscillations in instantaneous mode ZPE still occurs.

E. Phase space volume and quasiperiodicity

Why is it that the current implementation of TRAPZ has induced ergodic (RRKM) behaviour in the (otherwise non-ergodic) HNC system, but a slightly different implementation induced quasiperiodic limit-cycle behaviour in the (otherwise chaotic) Hénon–Heiles system while yet a third implementation preserved the chaotic behaviour of the Hénon–Heiles system?[27,33,34] The calculations here suggest that TRAPZ induces ergodic behaviour in molecular systems. Why then does the Hénon–Heiles system exhibit both ergodic and quasiperiodic behaviour for different versions of TRAPZ?

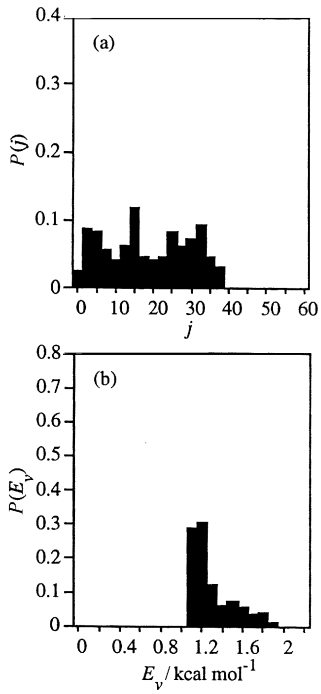

Fig. 8 Product dimer probability distributions for a TRAPZ ($\kappa_{\mathbf{WR}}$) ensemble of 200 trajectories, sampled around the linear equilibrium at an energy of 2.0 kcal mol^{-1} above classical threshold. (a) Angular momentum distribution of the product dimer ($\hbar$ units); and (b) vibrational energy distribution (kcal mol^{-1}).

1. Time reversibility. At first, it was thought that this effect was due to the time-irreversible nature of TRAPZ, which involves trajectories leaving the ZPE orbit tangentially [Fig. 1(b)] regardless of the incident angle [Fig. 1(a)]. Indeed, studies with a time-reversible form of TRAPZ, whereby trajectories leave at the same angle as they approach [Fig. 1(c)], have shown none of the quasiperiodic behaviour exhibited by the irreversible method. This was tested by two new versions of TRAPZ. The first required that trajectories leave the ZPE orbit at a fraction of the angle at which they were incident upon it:

$$\theta_{\text{out}} = \sigma\theta_{\text{in}}\,; \quad \text{for } \sigma > 0 \tag{31}$$

where θ_{in} and θ_{out} are the angles at which the trajectory approaches and leaves the ZPE orbit respectively. This is a generalisation of the time-reversible method described by Fig. 1(c), in the sense that earlier states of the system can be determined by inverting the equations of motion [including eqn. (31)] and back-integrating. The second method required trajectories leave the ZPE orbit at a constant angle, μ:

$$\theta_{\text{out}} = \mu$$

This is a generalisation of the irreversible method [Fig. 1(b)], since knowledge of the current state of the system cannot be used to determine the state of the system at some previous time.

Both methods were found to lead to limit cycle behaviour when trajectories were made to leave the ZPE orbit at small angles (σ, μ small), and no limit cycles were formed for greater outgoing angles (σ, μ large). This suggests that it is not the time-reversibility of the method, but the angle of exodus from the ZPE orbit, which is foremost the reason for limit cycle formation.

2. Phase space volume. We note that the current (Section II), and other, formulations of TRAPZ, are not canonical transformations and do not preserve phase-space volume. This can be seen by considering the Jacobian, which (for the full mapping) is

$$\frac{\mathrm{d}(\bar{Q}', \bar{P}')}{\mathrm{d}(\bar{Q}, \bar{P})} = (\beta')^{3N-6-v} \prod_{k=1}^{v} \lambda'_k$$

where

$$\lambda'_k = \frac{P'_k}{P_k}\,; \quad \text{for } k = 1, \ldots, v$$

This is generally not unity, and is either greater or smaller depending on the particular values of mode momenta. Since phase space volume is not conserved by the mapping, Liouville's theorem is also inapplicable.[39,52,53] This accounts for the unusual behaviour encountered[27] when the method was first tested on the two-mode Hénon–Heiles system,

$$H = \tfrac{1}{2}(P_1^2 + P_2^2) + \tfrac{1}{2}(\Omega_1^2 Q_1^2 + \Omega_2^2 Q_2^2) + Q_1^2 Q_2 - \tfrac{1}{3}Q_2^3 \tag{32}$$

Fig. 9 shows the time dependence of three small TRAPZ constrained elements of phase-space volume for this system. The volume used is the canonical four-form, $\Lambda^{(4)}_{1,2,3,4}$ which can be formulated as follows.[39] We take a point in phase space, (Q_1, Q_2, P_1, P_2), and four small displacement vectors, $(\delta_i Q_1, \delta_i Q_2, \delta_i P_1, \delta_i P_2)$ for $i = 1, \ldots, 4$:

$$\Lambda^{(2)}_{i,j} = \sum_{k=1}^{2} (\delta_i P_k \delta_j Q_k - \delta_i Q_k \delta_j P_k)$$

$$\Lambda^{(4)}_{1,2,3,4} = \Lambda^{(2)}_{1,2}\Lambda^{(2)}_{3,4} - \Lambda^{(2)}_{1,3}\Lambda^{(2)}_{2,4} + \Lambda^{(2)}_{1,4}\Lambda^{(2)}_{2,3} \tag{33}$$

This is an integral invariant of any unconstrained (classical) Hamiltonian system.[39] Fig. 9 shows that this is not the case for a TRAPZ system. The phase-space volume is dramatically

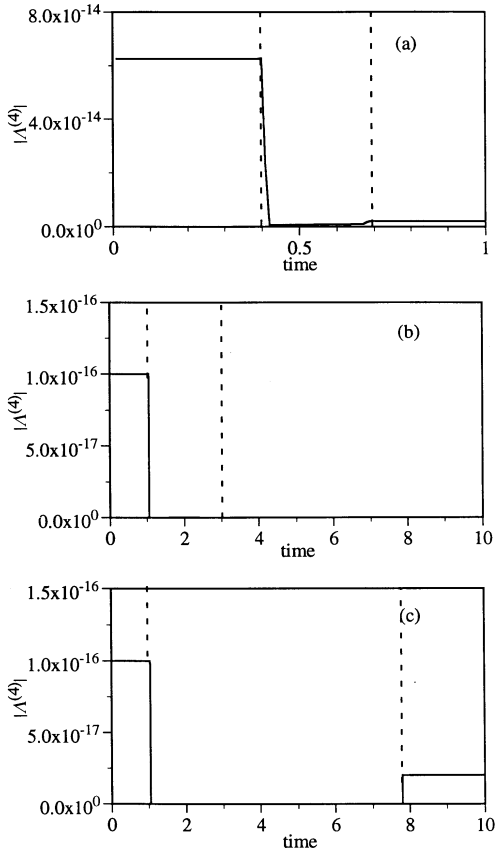

Fig. 9 Absolute value of the canonical 4-form [eqn. (33)], *vs.* time, for two different Hénon–Heiles systems. A mode violates between the dashed lines in each case, and no modes violate outside the lines. (a) A time-irreversible TRAPZ trajectory. (b) Another time-irreversible TRAPZ trajectory. (c) A time-reversible TRAPZ trajectory, but with the same intial positions and momenta as (b).

altered in between the dashed vertical lines, where one of the modes violates. Outside of these lines the system is unaffected by TRAPZ, since no mode is violating, and the phase space volume is constant.

Fig. 9(a) and (b) both show the volume dropping to zero (within numerical error) when the (time-irreversible) TRAPZ constraint is applied: TRAPZ has compressed the volume onto the ZPE orbit. In Fig. 9(a) some of this lost volume is reclaimed upon leaving the ZPE orbit, but in Fig. 9(b) it is not, and a limit cycle is formed. This compression of phase space in the Hénon–Heiles system, by TRAPZ, is closely linked to the formation of limit cycles and, particularly, in those cases where elemental volumes are not restored to non-zero values upon leaving the ZPE orbit. It is known that a space of zero *effective* volume *can never* be aperiodic. For example, any one-dimensional oscillator is totally periodic in the absence of external perturbations. Yet the same oscillator is also totally ergodic since its trajectory (Q, P) explores every point on its one-dimensional closed orbit.

The reductions in phase-space volume in the Hénon–Heiles system are thus closely linked to the way in which trajectories leave the ZPE orbits, and the formation of limit cycles is primarily dependent upon whether or not the outgoing angle is large enough to ensure sufficient reclamation of phase space volume. This is supported by Fig. 9(c), which shows a time-reversible system ($\sigma = 1$) corresponding to the same initial conditions as Fig. 9(b). In this case, some of the lost phase-space volume has been regained upon leaving the ZPE orbit.

No TRAPZ induced quasiperiodicity has yet to be observed in systems other than the Hénon–Heiles system.[27,34] This limit-cycle behaviour is unlikely to be exhibited when TRAPZ is implemented using the instantaneous modes of a system,

which are implicitly time dependent, but may well exist for studies with 'fixed' bases.

V. Conclusions

The TRAPZ method has been developed and generalised to include molecular systems of non-zero angular momentum, in such a way as to conserve total energy, linear and angular momentum. In essence, it involves making a small perturbation to the momentum of each vibrational instantaneous normal mode at the conclusion of each discrete time step, and corresponds to the minimum possible change in dynamics (forces) required to ensure preservation of ZPE.

For a study of the Al_3 cluster in the energy range 3–13 kJ mol^{-1} above the classical threshold and with $J = 0$, TRAPZ was found to preserve the RRKM behaviour of the classical system. TRAPZ rate coefficients were smaller than those found by classical-trajectory calculations, because TRAPZ does not allow unphysical routes to dissociation, but higher than those predicted by the BMH method.[45] A large portion of trajectories populate Al—Al stretching states with low vibrational-energy, freeing up more energy for the reaction coordinate and thus increasing the TRAPZ rate over the BMH rate. Most significantly, the TRAPZ rate coefficients are all less than the quantum RRKM coefficients, which are an absolute upper bound to the true rate coefficients for any ergodic system.

The TRAPZ product vibrational energy distribution is peaked at an effective threshold energy, higher than the true reaction threshold. This standardisation of final states seems to occur at the beginning of evaporation, and is related to increases in the probability of each vibrational mode being at ZPE. Despite this concentration of product vibrational energies at the low end of the spectrum, the product-energy lower bound itself is actually much higher than the true product ZPE, due to fluctuations in the instantaneous normal mode ZPEs at the beginning of monomer evaporation. The instantaneous normal mode ZPE can be as much as 35% higher than that for the isolated dimer, thus resulting in initial excessive pooling of mode energy, which is then retained throughout the rest of the dissociation process.

The TRAPZ product angular momentum distribution is also peaked at an effective threshold, resulting from the conversion of reactant bending-mode ZPE into non-zero dimer rotation. The $Al + Al_2$ potential is anisotropic only at short range, so no further interconversion of translational/vibrational/rotational energy or interconversion of orbital and dimer angular momenta can occur on separation. This could also be the result of over-constraining the reactant molecules, and may be remedied by modifying the method to treat reactant and transition molecules separately.

The effect of TRAPZ on a non-RRKM process (isomerisation of HNC) was also investigated. TRAPZ was found to lead to faster rates of decay and more ergodic (RRKM-like) behaviour. We postulate that this is caused by TRAPZ introducing *additional* non-linear coupling to the usual equations of motion, and hence destroying the invariant tori inherent in the classical system which are responsible for the non-ergodic isomerisation of HNC.

At first sight, there seems an apparent contradiction between this study and some of our earlier work on the Hénon–Heiles system in which *non*-ergodic (non-RRKM) limit-cycle behaviour[27] was observed. This paradox was resolved by noting that the TRAPZ method is a non-canonical transformation, since the Jacobian is generally not unity, and therefore does not preserve phase-space volume. Studies of the Hénon–Heiles model suggest that the limit cycles observed in earlier work[27] occur when the volume lost by an infinitesimal element colliding with the forbidden region, is not recovered upon leaving the ZPE orbit. This is due to the way in which trajectories leave the orbit, and not to the time-irreversibility of the method, since other variations of TRAPZ[27,34] do not exhibit this behaviour. No TRAPZ-induced quasiperiodicity has been observed in any system for which instantaneous normal modes were used.

Acknowledgements

This work is funded by an Australian Research Council Large Grant, and (for D.A.M.) an Australian Postgraduate Award. We thank Professor Huw O. Pritchard and Dr Wai-To Chan for providing computer code for the potential energy surface of HNC; and Dr Gilles H. Peslherbe, for supplying us with his BMH-modified version of VENUS96. K.F.L. thanks Jeanne Lee (Orica, formerly ICI Australia) for helpful and encouraging discussions.

References

1 D. L. Clark, and M. A. Collins, *J. Chem. Phys.*, 1987, **86**, 6871.
2 D. L. Clarke and M. A. Collins, *J. Chem. Phys.*, 1987, **87**, 5312.
3 Y. Guan and D. L. Thompson, *J. Chem. Phys.*, 1988, **88**, 2355.
4 D-H. Lu, W. L. Hase and R. J. Wolf, *J. Chem. Phys.*, 1986, **85**, 4422.
5 D-H. Lu, and W. L. Hase, *J. Phys. Chem.*, 1988, **92**, 3217.
6 D-H. Lu and W. L. Hase, *J. Chem. Phys.*, 1988, **89**, 6723.
7 A. J. Stace and J. N. Murrell, *J. Chem. Phys.*, 1978, **68**, 3028.
8 K. F. Lim, *J. Chem. Phys.*, 1994, **101**, 8756.
9 K. F. Lim, *J. Chem. Phys.*, 1994, **100**. 7385.
10 G. Lendvay and G. C. Schatz, *J. Chem. Phys.*, 1992, **96**, 4356.
11 T. Lenzer, K. Luther, J. Troe, R. G. Gilbert and K. F. Lim, *J. Chem. Phys.*, 1995 **103**, 626.
12 R. G. Gilbert, *Australian J. Chem.*, 1995, **48**, 1787.
13 N. S. Swamy and W. L. Hase, *J. Am. Chem. Soc.*, 1984, **106**, 4071.
14 J. A. Miller, *J. Chem. Phys.*, 1986, **84**, 6170.
15 L. A. M. Quintales, A. J. C. Varandas and J. M. Alvarino, *J. Phys. Chem.*, 1988, **92**, 4552.
16 M. R. Pastrama, L. A. M. Quintales, J. Brandao and A. J. C. Varandas, *J. Phys. Chem.*, 1990, **94**, 8073.
17 J. Davidsson and G. Nyman, *J. Chem. Phys.*, 1990, **92**, 2407.
18 G. Nyman and J. Davidsson, *J. Chem. Phys.*, 1990, **92**, 2415.
19 U. Wilhelmsson and G. Nyman. *J. Chem. Phys.*, 1992, **96**, 1886.
20 A. J. C. Varandas and J. M. C. Marques, *J. Chem. Phys.*, 1994, **100**, 1908.
21 A. J. C. Varandas, *Chem. Phys. Lett.*, 1994, **225**, 18.
22 J. M. Bowman, B. Gazdy and Q. Sun, *J. Chem. Phys.*, 1989, **91**, 2859.
23 R. Alimi, A. Garcia-Vela and R. B. Gerber, *J. Chem. Phys.*, 1992, **96**, 2034
24 G. H. Peslherbe and W. L. Hase, *J. Chem. Phys.*, 1994, **100**, 1179.
25 M. Ben-Nun and R. D. Levine, *J. Chem. Phys.*, 1994, **101**, 8768.
26 S. Kumar, N. Sathyamurthy and R. Ramaswamy, *J. Chem. Phys.*, 1995, **103**, 6021.
27 K. F. Lim and D. A. McCormack, *J. Chem. Phys.*, 1995, **102**, 1705.
28 Y. Guo, D. L. Thompson and T. D. Sewell, *J. Chem. Phys.*, 1996, **104**, 576.
29 D. Shen and H. O. Pritchard, *J. Chem. Soc., Faraday Trans.*, 1996, **92**, 1297.
30 D. L. Shen and H. O. Pritchard, *J. Chem. Soc., Faraday Trans.*, 1996, **92**, 4357.
31 K. F. Lim, *J. Chem. Soc., Faraday Trans.*, 1997, **93**, 669.
32 W. H. Miller, W. L. Hase and C. L. Darling, *J. Chem. Phys.*, 1989, **91**, 2863.
33 D. A. McCormack and K. F. Lim, *J. Chem. Phys.*, 1995, **103**, 1991.
34 D. A. McCormack, and K. F. Lim, *J. Chem. Phys.*, 1997, **106**, 572.
35 M. Hénon and C. Heiles, *Astron. J.*, 1964, **69**, 73.
36 D. W. Noid and R. A. Marcus, *J. Chem. Phys.*, 1977, **67**, 559.
37 D. W. Noid, M. L. Koszykowski and R. A. Marcus, *J. Chem. Phys.*, 1979, **71**, 2864.
38 M. D. Feit and J. A. Fleck, *J. Chem. Phys.*, 1984, **80**, 2578.
39 M. C. Gutzwiller, *Chaos in Classical and Quantum Mechanics*, Springer, New York, 1990.
40 S. E. Koonin and D. C. Meredith, *Computational Physics*, Addison-Wesley, Reading MA, 1st edn., 1990, p. 639.
41 A. P. Fordy, *Physica D*, 1991, **52**, 204.
42 M. Brack, R. K. Bhaduri, J. Law and M. V. N. Murthy, *Phys. Rev. Lett.*, 1993, **70**, 568.

43 D. A. McCormack and K. F. Lim, paper presented at Conference on the Dynamics of Molecular Collisions, Pacific Grove, USA, 1995; D. A. McCormack, Ph.D. Thesis, University of Melbourne, 1997.
44 G. H. Peslherbe and W. L. Hase, *J. Chem. Phys.*, 1994, **101**, 8535.
45 G. H. Peslherbe and W. L. Hase, *J. Chem. Phys.*, 1996, **104**, 9445.
46 T. D. Sewell, D. L. Thompson, J. D. Gezelter and W. H. Miller, *Chem. Phys. Lett.*, 1992, **193**, 512.
47 F. E. Budenholzer, M. Y. Chang and K. C. Huang, *J. Phys. Chem.*, 1994, **98**, 12501.
48 D. Shen, W. T. Chan and H. O. Pritchard, *J. Chem. Soc., Faraday Trans.*, 1996, **91**, 3747.
49 W. T. Chan, D. Shen and H. O. Pritchard, *J. Chem. Soc., Faraday Trans.*, 1995, **91**, 1717.
50 T. Keyes, *J. Phys. Chem. A*, 1997, **101**, 2921.
51 W. H. Miller, N. C. Handy and J. E. Adams, *J. Chem. Phys.*, 1980, **72**, 99.
52 H. Goldstein, *Classical Mechanics*, Addison-Wesley, Reading, 1980.
53 T. W. B. Kibble, *Classical Mechanics*, Longman, London, 3rd. edn., 1985.
54 D. J. Evans and G. P. Morriss, *Comput. Phys. Rep.*, 1984, **1**, 297.
55 R. A. Edberg, D. J. Evans and G. P. Morriss, *J. Chem. Phys.*, 1986, **84**, 6933.
56 C. Eckart, *Phys. Rev.*, 1934, **46**, 383.
57 A. Sayvetz, *J. Chem. Phys.*, 1939, **6**, 383.
58 *Dynamics of Molecular Collisions*, ed. W. H. Miller, Plenum Press, New York, 1976.
59 J. H. Beynon and J. R. Gilbert, *Applications of Transition State Theory to Unimolecular Reactions*, Wiley, New York, 1984, p. 85.
60 M. J. Pilling, I. W. M. Smith, *Modern Gas Kinetics: Theory, Experiment, and Application*, Blackwell, Oxford, 1987.
61 J. I. Steinfeld, J. S. Francisco and W. L. Hase, *Chemical Kinetics and Dynamics*, Prentice Hall, Englewood Cliffs, 1989.
62 W. L. Hase, R. J. Duchovic, X. Hu, A. Komornicki, K. F. Lim, D.-H. Lu, G. H. Peslherbe, K. N. Swamy, S. R. Vande Linde, A. Varandas, H. Wang and R. J. Wolf, *Quantum Chem. Program Exchange Bull.*, 1996, **16**, 43.
63 W. L. Hase and D. Buckowski, *Chem. Phys. Lett.*, 1980, **74**, 284.
64 J. N. Murrell and S. Carter, *J. Mol. Spectrosc.*, 1982, **93**, 307.
65 S. J. Klippenstein and R. A. Marcus, *J. Phys. Chem.*, 1988, **92,** 5412.
66 J. Yu and S. J. Klippenstein *J. Phys. Chem.*, 1991, **95**, 9882.
67 S. J. Klippenstein, *J. Chem. Phys.*, 1991, **94**, 6469.
68 S. J. Klippenstein, *J. Chem. Phys.*, 1992, **96**, 367
69 R. G. Gilbert. and S. C. Smith, *Theory of Unimolecular and Recombination Reactions*, Blackwell, Oxford, 1990.
70 C. Schlier, *J. Chem. Phys.*, 1995, **103**, 1989.
71 G. Z. Whitten. and B. S. Rabinovitch, *J. Chem. Phys.*, 1963, **38**, 2466.
72 G. Z. Whitten and B. S. Rabinovitch, *J. Chem. Phys.*, 1964, **41**, 1883.

Paper 8/08024K